Phys Chem Minerals (1993) 20:86–90

PHYSICS AND CHEMISTRY OF MINERALS

Laser-Heated Diamond Anvil Cell Experiments at High Pressure: Melting Curve of Nickel up to 700 kbar

P. Lazor, G. Shen, and S.K. Saxena

Geochemistry Program, Department of Mineralogy and Petrology, P.O. Box 555, Uppsala University, S-751 22 Uppsala, Sweden

Received August 20, 1992 / Revised, accepted March 2, 1993

Abstract. Laser-heated experiments in a diamond anvil cell have been performed on high pressure melting of nickel up to 700 kbar. The laser heating system consists of diamond anvil cell, Nd:YAG and argon lasers, spectrograph with diode array, computer with software, CCD camera with monitor and optics. Experiments on melting of tungsten, nickel and platinum at 1 bar outside the diamond anvil cell and melting of nickel below 80 kbar in the cell were carried out to check the system for pressure and temperature measurements. The results show that for solid pressure medium the uncertainties in measurements of pressure at the experimental spot vary between ± 5 kbar at 100 kbar and ± 25 kbar at 660 kbar. Spectroradiometrically determined temperature is reliable within ± 70 K. Melting was detected in situ by visual observation. The melting point of nickel at 660 kbar has been found to be 2557 ± 66 K.

Introduction

The laser-heating technique combined with pressure generation in a diamond anvil cell (DAC) provides a unique opportunity to study high pressure and high temperature physical and chemical properties of matter, which are of great importance for understanding the nature of our planetary system, especially the earth. The importance is reflected in a growing number of studies involved in this field of study. (Williams et al. 1987; Boehler et al. 1990; Knittle and Jeanloz 1991; Heinz and Sweeney 1991). Since the pioneering work of Ming and Bassett (1974) the technique has been considerably improved though the basic idea remains the same. More powerful and stabilized lasers are now available which permit heating of the samples to high and well defined temperatures. Spectroradiometry with multichannel detectors have become common and reliable tools for temperature determination.

With such instruments the DAC technique is especially suitable for high pressure melting experiments on possible constituents of the earth's interior. In this regard iron and nickel are considered important. Boehler et al. (1990) have studied the iron melting but such a study on nickel is still lacking. We present here melting of nickel up to 700 kbar. According to Liu (1982), nickel is assumed to be the third (4.68 w.%) and the second (5.14 w.%) most abundant element in the inner and outer core, respectively. Melting curve of nickel has been measured by Strong and Bundy (1959) up to 60 kbar in a piston-cylinder apparatus.

Experimental Technique

The Equipment

The laser heating system shown in Fig. 1 is based on the one developed by Boehler et al. (1990). The heating Nd:YAG laser (Coherent) operates in CW TEMoo mode at wavelength 1064 nm. The laser provides maximally 30 W of vertically polarized light with a feed-back controlled stability better than 0.5% peak-to-peak. The beam from the laser is expanded in $3\times$ beam expander BE to decrease the power density on subsequent optics and to improve the focussing ability. Continuously variable attenuator changes the power of the beam reaching the sample in the cell without disturbing the thermal equillibrium of the Nd:YAG laser. It consists of a rotatable half plate $\lambda/2$ and a polarizing beamsplitter cube P. By rotation of the plate the ratio between the light passing the cube and the deviation can be continuously changed. Lenses L1 and L3 (50 mm focal length) focus the Nd:YAG and argon laser beams on the sample. Both beams can be focussed to a spot of about 20 μm in diameter. Because of the antireflection coatings on the optics and the high transmission of the attenuator as much as 90% of the maximum laser power can reach the sample. The reflecting objective ($15\times$, w.d. 25 mm) is used to collect the thermal radiation of the sample. The objective is free of refractive elements, hence free of chromatic aberration. Filter F1 cuts the reflected beam of the Nd:YAG laser from the sample surface to protect the subsequent electronics devices. Lens L2 (250 mm focal length) focusses the light on the entrance pinhole of the spectrograph and, by mean of beamsplitter BS (10R/90T), on the CCD camera. The 50 μm in diameter pinhole of the spectrograph collects the radiation from an area of 3 μm in diameter of the sample. The interference filter F2 transmits only the Ar laser light (488 nm) reflected from the sample surface. This light is used for the illumination

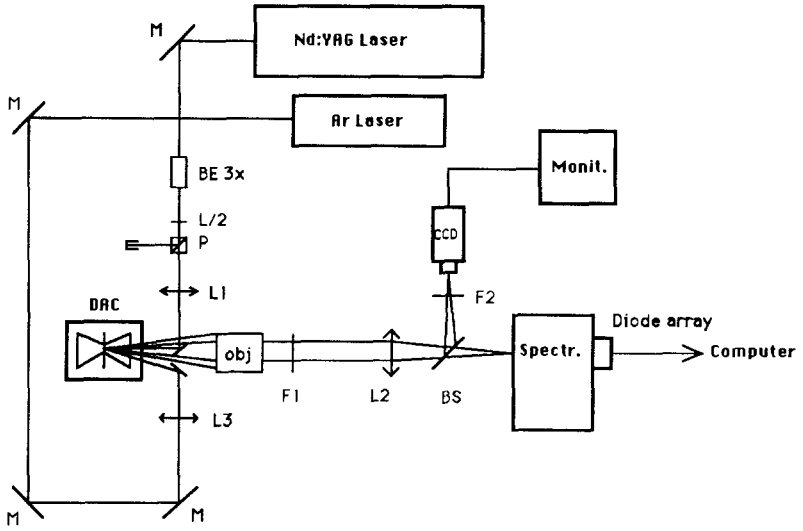

Fig. 1. Plan of the laser heating system. BE – beam expander, $\lambda/2$ – half plate, P – polarizing beamsplitter cube, L1, L2, L3 – lenses, M – mirrors, BS – beamsplitter, F1, F2 – filters, obj – reflecting objective, DAC – diamond anvil cell

of the sample during the experiment. The optical system is almost free of chromatic aberration which reduces the error in temperature determination. Lens L2 eliminates the light dispersion caused by the diamond in the cell. On the monitor attached to the CCD camera, details as small as one micrometer can be resolved in reflected Ar laser light. The spectrograph with linear photodiode array transforms the light coming from the cell to spectrum converted by a computer program into the current P–T conditions in the cell.

The megabar diamond anvil cell developed by Mao and Bell (Jephcoat et al. 1987) has been used for our experiments. Diamonds are standard Drukker type IA with 0.45 mm diameter flat culets.

System Calibration

Several experiments were carried out to check pressure and temperature determination in our system. Polished platinum and tungsten foils were melted under a flow of argon at 1 bar outside the diamond anvil cell. Using literature values for wavelength dependence of emissivities (Cabannes 1967; De Vos 1954) the melting temperatures 3671 ± 37 K for tungsten and 2041 ± 33 K for platinum were found in agreement, respectively with the published temperatures of 3683 ± 20 K and 2045 K.

Another test of the system was the melting of nickel below 80 kbar. The temperatures of melting were determined by Strong and Bundy (1959). The results showing consistency of both measurements are discussed here together with high pressure melting of nickel.

Sample Preparation

Pure nickel (99.98%) in the form of 10–15 μm thick polished foil was used for the experiment. A stainless steel T301 gasket with 300 μm diameter hole formed a pressure chamber. Prior to an experiment the gasket was indented between diamond anvils with pressure at the center about 100 kbar. The gasket thickness before indention was 250 μm, after indention 100–150 μm.

The parallel alignment of the diamond operating faces was achieved by adjusting (rotation) diamond bearing rockers while observing the faces in transmitted light under microscope before mounting the sample. The unparallelism of the faces is recognized by number of parallel coloured stripes that appear due to interference of light. We rotated one or both rockers until the number of stripes is three maximally; a sufficient degree of parallelism for the experimental pressure range. The alignment was rechecked after indention and before each mounting of the sample.

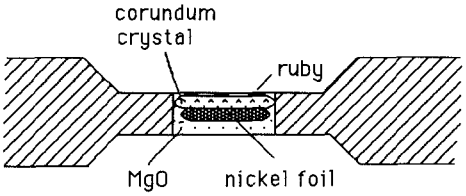

Fig. 2. Sample assemblage for melting of nickel. The diameter of the sample is about 250 μm, the thickness 10–15 μm

In our earlier experiments we had used MgO as a pressure medium and taken the temperature of melting as soon as the melting was observed. Once the melting begins, a distinct reaction with the powder can be observed. In order to avoid this, we followed the method suggested by Boehler et al. (1990) who used a corrundum disk on the top of the sample as the isolator. The use of such a disk eliminates the possibility of any significant reaction between the sample and the disk which is much less reactive than the powder.

The arrangement of the chamber assemblage is shown in Fig. 2. The nickel foil was placed on a layer of periclase powder and a disc of colorless corundum was put over it. Then small ruby chips were spread over the assemblage.

Pressure Determination

For the pressure determination the calibrated pressure shift of ruby R1 fluorescent line was used (Mao et al. 1978). The argon laser beam (488 nm) was focussed by lens L3 (Fig. 1) on one of the ruby chips put along with the sample in the chamber (Fig. 2). The fluorescent light of illuminated ruby was collected by the objective, passed to the spectrograph and the position of R1 line found in the spectrum. Only a circular area with diameter of 3 μm was sampled by the spectrograph to get one pressure value. This reduced errors in pressure determination resulted from the presence of pressure gradient in the chamber. The pressure was determined at room temperature. However, prior to the measurement, we heated a chosen spot by laser to mechanically relax sample assemblage before the real melting experiment. The pressure dropped up to 16% of the initial unrelaxed value. We repeated the measurement after each melting experiment. The drop varied in between 1% to 3%. All experimental spots were chosen either in the very vicinity of the ruby chips or right below them. The errors given in Table 1 reflect the magnitude of pressure gradient in the chamber and the

Table 1. Experimental data on p–T of melting of nickel

1. Pressure at 298 K (kbar)	2. Thermal pressure (kbar)	3. Melting pressure (kbar)	4. Measured temperature (K)	5. Correc. for time averag. (K)	6. Correc. for spatial averag. (K)	7. Melting temp. (K)
1	0	1	1690±18	50±10	5± 3	1745±31
30± 5	20	50± 5	1830±22	50±20	15± 5	1905±47
50± 5	20	70± 5	1892±25	50±20	15± 5	1969±50
62± 5	20	82± 5	1905±17	50±20	15± 5	1995±42
111±10	22	133±10	2024±25	50±20	15± 5	2099±50
117±10	22	139±10	2042±26	50±20	20± 8	2122±54
119±10	21	140±10	1986±22	50±20	15± 5	2070±47
213±15	24	237±15	2195±24	50±20	20± 8	2273±52
224±15	23	247±15	2137±27	50±20	20± 8	2200±55
280±20	24	304±20	2186±19	50±20	20± 8	2268±47
302±25	25	327±25	2241±18	50±20	25±11	2328±49
369±20	25	394±20	2307±24	50±20	25±11	2394±55
433±25	26	459±25	2338±32	50±20	25±11	2425±63
490±30	27	517±30	2408±28	50±20	25±11	2498±59
632±25	27	659±25	2465±34	50±20	25±11	2557±65

incidental pressure drop during melting experiment. At the pressure of 660 kbar in the center of the chamber the pressure difference between the center and the edge was 140 kbar.

Procedure and Melting Detection

We have found that visual observation is a convenient method for reliable detection of the moment when melting happens. Beside this we look for a change of the slope of laser power/sample temperature function, a supplementary evidence of melting. However, the method of watching requires a clear surface to see which is not the case if a sample is very hot (2000–2300 K and more, depending on the emissivity); the thermal radiation blocks the view. To overcome the problem, we put narrow bandpass (488±1 nm) interference filter in front of the CCD camera and illuminate the nickel surface with defocussed argon laser light (488 nm) during an experiment. Then in this reflected light we watch the surface subjected to increased heating from the Nd:YAG laser. We increase the power of the laser in steps, continuously taking spectra in between and waiting few seconds to ensure if upward fluctuations of temperature could reach melting point. If this happens, the corresponding temperatures are recorded and corrected for temporal and spatial averaging (described below). The result is considered to be a melting temperature at a given pressure. We continue to increase laser power until the occasional fluctuational melting changes into continuous convective movement. This is to discern between possible recrystallization and real melting. Another confirmation of melting is the appearance of its characteristic roundish features. The melting is reversed few times (between 2 and 4 for various spots) to insure repeatibility and obtain an error estimation.

Using the method described above for melting of tungsten at 1 bar we clearly observed marked and extensive recrystallization around 2700 K, pre-melting softening and shaking followed by occasional fluctuational melting and finally continuous melting up to 4200 K.

Melting Temperature Determination

The spectral response of the optical system is found by means of NIST calibrated tungsten-halogen lamp. The thermal radiation entering the spectrograph is dispersed by 300 gr/mm grating across the photodiode array and spectrum from 600 nm to 900 nm is received. After the correction for spectral response of the optical system the spectrum is fitted by a least squares method to Wien's approximation of Planck's radiation function. Wavelength dependence of emissivity is taken from Cabannes (1967) with data from 5 different resources all of which are consistent with the slope of the curve at 750 nm. However, the absolute magnitudes of emissivity at 750 nm are scattered. In Weast (1989) the absolute value of emissivity at 650 nm is 0.36. From the data we chose the slope with a value of ε_1 as $-2*10^{-4}\,\mathrm{nm}^{-1}$ and $emis_{750}$ as 0.35 ± 0.02 which are used for expressing the wavelength dependence of emissivity as

$$emis = emis_{750} + \varepsilon_1 * (\lambda - 750\ \mathrm{nm})$$

where λ is wavelength in nanometers. The assumed interval for $emis_{750}$ resulted in an additional error in temperature ranging from ±5 K at 1800 K to ±10 K at 2600 K. At the present state of the theory and available data it was difficult to consider pressure and temperature dependence of emissivity. Generally, small dependence is believed in. Neglecting the dependence of emissivity on wavelength results in underestimating the melting temperature from 75 K at 1800 K to 145 K at 2600 K.

Since we use diode array which is not intensified, the time to collect one spectrum for temperature range 1600–3000 K is between 5.2 s to 0.16 s. The typical time constant of temperature fluctuations due to laser power instability of only a tens of milliseconds results in temporal averaging of the temperature. To find the correction for the averaging, a series of quick consecutive measurements of temperature were run for tungsten and platinum. Figure 3a,b shows the typical results. For tungsten at 3200 K temperature fluctuated within ±80 K with integration time of 40 ms for each spectrum. For platinum at 1850 K the fluctuations reached ±34 K with time averaging of 2.5 s. Using the method of approaching and catching the first "fluctuational" melting described above we added 50 K with an error of ±20 K to the measured averaged melting temperatures assuming 10–25 K above the melting point being needed to cause observable change in surface texture. The value is in accordance with melting point repeatibility and our experimental experience.

To avoid large temperature gradients within the sampled area Nd:YAG laser beam is focussed only to a degree necessary for achieving desired temperatures. Focussing or defocussing is accomplished by small movements of the lens L1 along its optical axis. The diameter of the hot spot may be varied between 25 and 50 μm at various pressures. To see how well the temperatures are defined within the scanned circle area, two measurements of temperature profiles were conducted. For temperatures 2175 K and 2050 K in the center of the hot spot, the gradients of 17 K/μm and 23 K/μm were found as shown in Fig. 4. The sample was platinum with

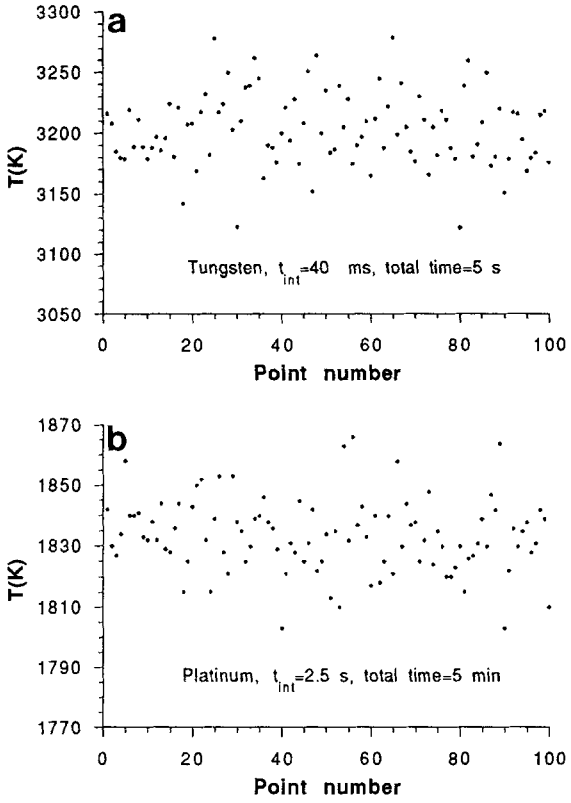

Fig. 3a, b. Typical temperature fluctuations resulting from laser power instability. **a** tungsten; **b** platinum

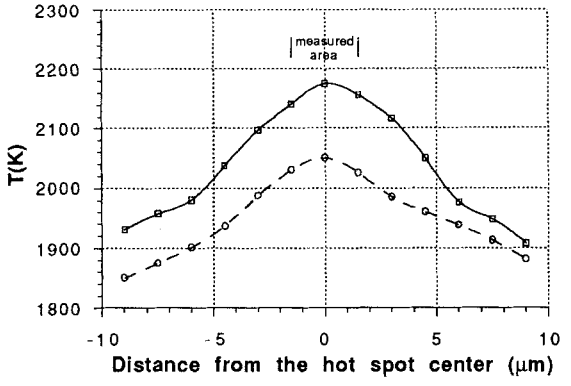

Fig. 4. Temperature profiles for platinum at 146 kbar with periclase as the pressure medium

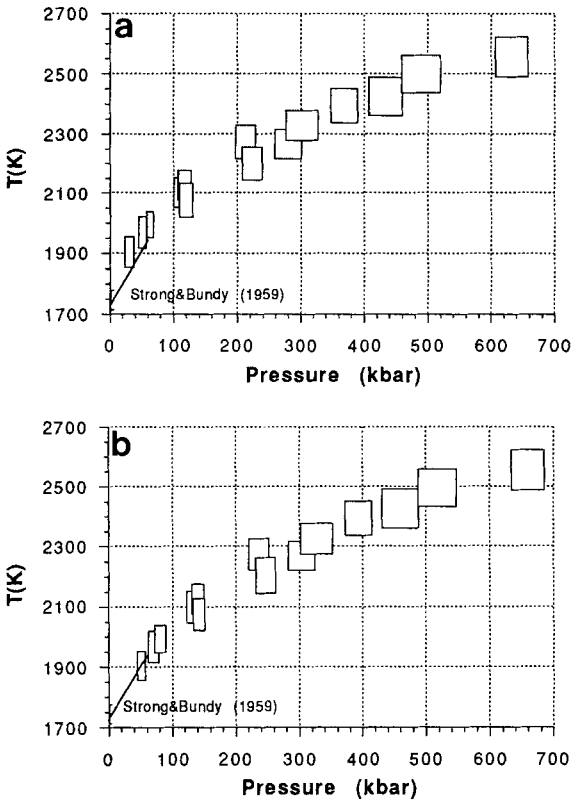

Fig. 5. a Melting curve of nickel. The pressure is the measured pressure from ruby scale after quenching of the sample. **b** Melting curve of nickel with estimated thermal pressure. See text for the method

periclase as the pressure medium at 146 kbar. Boehler et al. (1990) measured a maximum gradient of 15 K/μm for iron under argon pressure at 300 kbar and 2250 K. We use the temperature profile data to correct measured melting temperatures for spatial averaging. The linear increase of gradient with temperature is assumed to lie within the experimental temperature range. The magnitude of given errors results from the effect of possible misalignment of the hot spot center in the sample and the center of the spectrograph pinhole. This can happen due to a local change in laser power absorption across the sample surface.

Results and Discussion

Table 1 shows the experimental results. The melting phase equilibrium curve is shown in Fig. 5. The melting at 1 bar was carried out outside the diamond anvil cell under the flow of argon to prevent an oxidation of the sample. In the first column of the table, we report the pressure as found from the ruby scale for the quenched sample. As yet, a suitable experimental or theoretical technique to determine the pressure at the temperature of the experiment does not exist. Below we present a method of estimating the thermal pressure which must be considered only as approximate. Melting points at 30, 50 and 62 kbar lie at systematically higher temperatures than those of the melting curve of Strong and Bundy (1959). However, rather than considering this as a systematic error in our or in the previous measurements, we ascribe the difference to the thermal pressure built up in the cell during heating which we did not take into account previously. Considering the central values of our data, thermal pressure of a magnitude of 20 kbar would yield the agreement between the two sets of data. This value is reasonable as indicated from the calculations performed by Heinz (1990) on thermal pressure in the laser heated diamond anvil cell. Assuming typical, pressure and temperature independent values for coefficients of thermal expansivity and isothermal bulk modulus, a temperature difference of 2000 K and Poisson's ratio of 0.25, he calculated thermal pressures in the range of 20–80 kbar for various temperature profiles. Considering the upper limits of our low pressure data, we get a possible thermal pressure between 0 and

35 kbar. Column 2 in Table 1 contains data on thermal pressure calculated with the assumption of 20 kbar as thermal pressure at a pressure of 50 kbar for the quenched sample. Product of thermal expansion and bulk modulus coefficients was assumed as constant; only the effect of rising temperature was taken into the account

$$P_{th} = 20 \text{ kbar} * \frac{T_m - 300 \text{ K}}{1956 \text{ K} - 300 \text{ K}}$$

1956 K is the mean value of melting point temperatures at 30, 50 and 62 kbar. T_m is melting point temperature at a given pressure.

As found out from the pressure measurements significant pressure gradient develops inside the chamber with the solid pressure transmitting medium. The effect of shear stress on melting is not known and was not considered here.

Summary

Our experiments and results show that the newly created laser heating system is quite functional and reliable.

We have considered the possible effects which influence the precision of the temperature and pressure measurements. Particular care and attention have been paid to temperature determination. According to our 1 bar and low pressure melting results there is no large systematic error in the function of our system spectral response.

The low pressure data indicate significant values of thermal pressure in the sample chamber due to laser heating. Pressures obtained in this work are approximate and require additional studies. We postpone a consideration of retrieving thermodynamic data on nickel until we can estimate the thermal pressure with a greater precision.

Acknowledgments. Thanks are due to R. Boehler, Y. Fei and H.K. Mao who helped us in establishing our laboratory and shared their experience with us. We also had important discussions with J.F. Shu and D. Heinz. The work has been supported financially by grants from the Swedish Natural Science Research Council (NFR).

References

Boehler R, Bargen N von, Chopelas A (1990) Melting, thermal expansion, and phase transitions of iron at high pressures. J Geophys Res 95:21731–21736

Cabannes F (1967) Facteurs de réflexion et d'emission des metaux. J Phys 28:235–248

De Vos JC (1954) A new determination of the emissivity of tungsten ribbon. Physica 20:690–714

Heinz DL (1990) Thermal pressure in the laser-heated diamond anvil cell. Geophys Res Lett 17:1161–1164

Heinz DL, Sweeney JS (1991) A laser heating system that stabilizes and controls the temperature: Diamond anvil cell applications. Rev Sci Instrum 62 (6):1568–1575

Jephcoat AP, Mao HK, Bell PM (1987) Operation of the megabar diamond anvil cell. In: Ulmer GC, Barnes HL (eds) Hydrothermal experimental techniques. Wiley, New York, pp 469–506

Knittle E, Jeanloz R (1991) The high-pressure phase diagram of $Fe_{0.94}O$: A possible constituent of the Earth's core. J Geophys Res 96:16169–16180

Liu L (1982) Speculations on the composition and origin of the Earth. Geochem J 16:179–198

Mao HK, Bell PM, Shaner JW, Steinberg DJ (1978) Specific volume measurements of Cu, Mo, Pd and Au and calibration of the ruby R1 fluorescence pressure gauge for 0.06 to 1 Mbar. J Appl Phys 49:3276–3283

Ming LC, Bassett WA (1974) Laser heating in the diamond anvil press up to 2000° C sustained and 3000° C pulsed at pressures up to 260 kilobars. Rev Sci Instrum 9:1115–1118

Strong HM, Bundy FP (1959) Fusion curves of 4 Group-VIII metals to 100,000 atmospheres. Phys Rev 115:278–284

Weast RC (1989) CRC Handbook of Chemistry and Physics 69, p 405

Williams Q, Jeanloz R, Bass J, Svendsen B, Ahrens TJ (1987) The melting curve of iron to 250 gigapascals: a constraint on the temperature at the Earth's center. Science 236:181–182